Structural behaviour of beam to concrete-filled elliptical steel tubular column connections

J. Yang, T. Sheehan, X. Dai & D. Lam

School of Engineering, University of Bradford, Bradford, UK
E-mails: j.yang17@bradford.ac.uk, t.sheehan@bradford.ac.uk, x.dai@bradford.ac.uk, d.lam1@bradford.ac.uk

ABSTRACT

Elliptical Hollow Sections (EHSs) have been utilized in construction recently because of their visual appearance as well as the potential structural efficiency owing to the presence of the two principle axes. However, little information currently exists for the design of beam to elliptical column connections, which is an essential part of a building structure. Thus, to ensure the safe and economic application of EHSs, a new research project has been initiated. Rotation behaviour of simply bolted beam to concrete-filled elliptical steel column connections was investigated experimentally. Various joint types were considered and the benefits of adopting core concrete and stiffeners were highlighted. This paper covers the experimental studies and simulation of the connections using the ABAQUS standard solver. Comparisons of failure modes and moment vs. rotation relationships of the connections between numerical and experimental results were given. Good agreement has been obtained and the developed finite element model was therefore adopted to conduct a preliminary parametric study to explore the effect of critical parameters on the structural behaviour of beam to concrete-filled elliptical column connections.

Keywords: Concrete-filled columns; Elliptical hollow section; Beam to column connections; Finite element modeling.

1 Introduction

Concrete-Filled Steel Tubular (CFST) columns are well-known for their superior structural properties due to the mutual complementation of the steel tube and the concrete core. The most common cross-sectional shapes of CFST columns are circular, square and rectangular. A new range of Elliptical Hollow Sections (EHSs) has been made available recently by the manufacturing industry, which adds diversity to the sectional shape and fulfils the aesthetics demand by designers. However, limited information exists to enable safe and economic design of EHS components/connections in structures, which might limit its widespread application. Efforts have been made on investigating the structural behaviour of elliptical columns [1, 2], beams [3], welded truss EHS connections [4, 5]. Zhao and Packer [1] experimentally investigated both unfilled and concrete-filled EHS stub columns filled with normal concrete and self-consolidating concrete. According to the obtained results, they drived the yield slenderness limit which is used to identify occurrence of local buckling of steel hollow sections subjected to axial compressive force for carbon steel EHS based on the equivalent rectangular hollow sections (RHS). They also extended the above concept and

mehod to predict the load carrying capacity of concrete-filled EHS stub columns and good prediction was generated by using procedures in Eurocode 4. Dai and Lam [2] investigated the axial compressive behaviour of short concrete-filled EHS columns by using ABAQUS finite element analysing (FEA) software and an improved confined concrete stress-strain model was proposed for concrete-filled EHS stub columns. Typical failure modes, static bearing capacities and load versus end shortening relationships of the composite stub columns obtained by the finite element analysis were verified against experimental observations. The comparison and analysis indicated the FEA method was reliable in prediction the basic structural behaviour of concrete-filled EHS stub columns under compression. Static strength of axially loaded EHS X-joints with brace members welded to the narrow sides of the EHSs has been studied experimentally and numerically by Shen et al [4]. In their study, both brace member compression tests and tension tests were performed. They found that this type of EHS X-joint could be related to relevant circular hollow section X-joints. Despite the above mentioned attempts of investigation on EHS and those not specified provided herein, large gaps still exist in research. Beam to concrete-filled elliptical column connections, which are essential in framed structures, remain unfamiliar to designers. The fabrication of such connections could be complicated and cumbersome owing to the curved face of the column. Fin plate connections have been widely adopted owing to the merits of easier erection, rapid construction and lower cost. Jones [6] studied the behaviour of single-sided fin plate to steel tubular columns loaded by tensile and shear force. Parameters including column cross-section shape (CHS and RHS), column and fin plate thickness, concrete infill, elevated temperatures and lever arm were considered. In this study, failure modes including fracture of the fin plate and tearing out of the tube around the welds were observed, deformation limit of 3% of the tube width for hollow tubes in CIDECT Guide was re-evaluated and proved to be inadequate to extract the ultimate strength of the connections. In addition, concrete infill was observed to significantly increase the capacity of connections over empty ones and specimens with CHS were found to have greater strength than similarly proportioned RHS ones. However, this study only focus on isolated fin plate with column connections regardless of bolts that linking beams to the connections and also the moment behaviour of the connections was not explored especially when large beam rotation occurred. A series of double-sided fin plate beam-column connections considering different joint assemblies was investigated by Lam & Dai [7] through a numerical modelling technique, aiming to investigate their moment-rotation behaviour. Connections with and without concrete core and stiffener plates were studied. The studied joint types are illustrated in Figure 1, from type-AC to DC. An experimental study [8] was carried out to verify the obtained preliminary findings and also to provide better understanding of the structural behaviour of these joints, including an additional joint type-EC (Fig. 1, EC) which considered an embedded stiffener plate in the major axis direction of the EHS column. Corresponding connections with EHS columns, i.e. without concrete in-fill, were also tested to highlight the benefit of using the concrete infill. This paper herein presents the experimental program and

details of a Finite Element (FE) model for the simulation of the experiments on concrete-filled joints. Preliminary parametric numerical results based on the verified FE model are given to highlight the effect of critical parameters on the structural behaviour of beam to concrete-filled elliptical column connections.

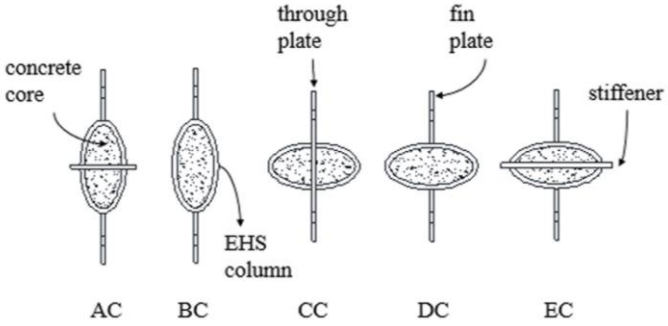

Figure 1. Joint types.

2 **Description of experimental program**

2.1 *Test arrangements*

Details of the experiments can be found in the previous paper [8], so only a brief summary is given in this section. A total of ten specimens (of which five are connections with a concrete core in the column and the other five are corresponding to hollow connections) were tested to failure with the column under a constant downward compressive force and the beams subjected to upward concentrated forces at the beam ends, replacing the slab-floor load that would occur in a real structure. Three hydraulic actuators were employed to exert these forces. Test arrangement and a typical beam to elliptical column specimen is shown in Figure 2 in which some dimensions of the connection are also illustrated. All EHS columns (200 × 100 × 5mm, 1500 mm in length, mean measured dimensions are listed in Table 1) were made of S355 steel with a tested average yield strength of 355.3 MPa and an ultimate strength of 522.1 MPa, respectively; fin plates and stiffener plates were made of S275 steel with tested yield strength and ultimate strength of 333.1 MPa and 444.5 MPa, respectively; elastic modulus was 205 GPa. Steel coupon tests were conducted in accordance with BS EN 6892-1 [9]. The unconfined average cube strengths of the infilled concrete (C30) were 37 MPa on 28 days and 42 MPa on the test dates. M20 Gr. 8.8 bolts (for type-D, DC, E, EC connections, where “type-D”, for example, means type-DC connection without infilled concrete) or Gr. 10.9 bolts (for type-A, AC, B, BC, C, CC connections) were used to connect the beams (305 × 127 × 48 UB, 900 mm in length) to the fin plates (220 × 110 × 10 mm), while the fin plates were welded to the external faces of the EHS columns using 6mm fillet welds. Bolt holes in both fin plates and through plate had a diameter of 22 mm. Stiffener plates/through plates (10 mm in thickness) ran through either the minor or major axes of the EHS columns with an extended length of 20 mm on each side. Vertical deflections of the beams and lateral deflections at the positions of the top and bottom bolts were measured by LVDTs during tests, to calculate rotations of each connection.

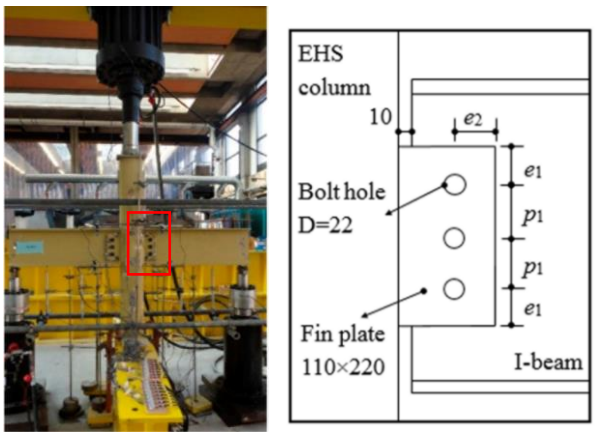

Figure 2. Test arrangements & Planed connection dimensions (e_1=50, e_2=50, p_1=60; mm).

Table 1. Mean measured dimensions of EHS columns (mm).

Specimen ID	$2a \times 2b \times t$ mm × mm × mm	L mm
Joint-A	198.43 × 99.52 × 5.05	1500
Joint-AC	198.60 × 101.89 × 4.97	1499
Joint-B	200.01 × 101.51 × 4.92	1487
Joint-BC	198.47 × 101.57 × 5.01	1498
Joint-C	198.50 × 100.50 × 4.88	1498
Joint-CC	198.21 × 101.42 × 5.02	1498
Joint-D	197.78 × 102.03 × 4.54	1497
Joint-DC	198.50 × 101.62 × 5.05	1500
Joint-E	197.82 × 102.10 × 4.75	1495
Joint-EC	198.11 × 101.58 × 5.17	1495

2.2 *Test results*

Summarized moment vs. rotation curves were illustrated in Figure 3, where the moment of each fin-plate connection is equal to the force at the beam end (recorded automatically by a data logger) multiplied by the functional distance (0.8 m) from the loading point to the rotation center. Curve “ECR” represents the result of a repeat test of concrete-filled type-EC connection, replacing M20 Gr. 8.8 bolts by M20 Gr. 10.9 bolts after the bolts fractured in the initial test. To improve the clarity of the comparison between the curves, only the phases before the failure points were plotted in this figure. The initial stage of the curves was found to be linear, and the slope was determined by the friction force that existed between the fin plates, beam webs and bolts. Slippage occurred in all cases before the bolt shanks touched the edges of bolt holes. The duration of this phase varied owing to the 2 mm clearance between the bolt shanks and holes. With the increase of rotation, slopes of the curves increased especially for concrete-filled column connections. The reason is that the top flange of each beam touched the EHS column face at some stage during the tests, while the transverse stiffness of the EHS was significantly enhanced by the core concrete. Summarized failure moment and the

corresponding rotations are listed in Table 2. The main findings in regards to the moment capacity are: 1) the moment resistance of simply bolted fin plate connections can be improved considerably by infilling concrete to the EHS column, enhancing moment resistance by a factor ranging from 1.91 to 5.19; 2) the minor axis through plate connection, type-CC, had much higher stiffness and better moment capacity and is thus to be recommended for minor axis beam to EHS column connections.

Typical failure modes of connections with hollow columns and concrete-filled columns are illustrated in Figure 4 (a) and (b), respectively. For all joint assemblies, connections with hollow EHS columns failed by inward local buckling although stiffeners were used in some cases. However, this phenomenon was eliminated by using core concrete. Large concave (in the upper portion of the connection, caused by direct compression of beam flange) or convex (in the lower portion, caused by tensile force transferred from fin plates) deformations that had occurred in the hollow columns were prevented when concrete infill was employed. Consequently, bolts fractured (shear failure) at the final stage of the tests. In contrast to the other hollow column specimens, the through plate connection, type-C, failed by bolt shear failure owing to the contribution of the through plate to the transverse stiffness of the connection.

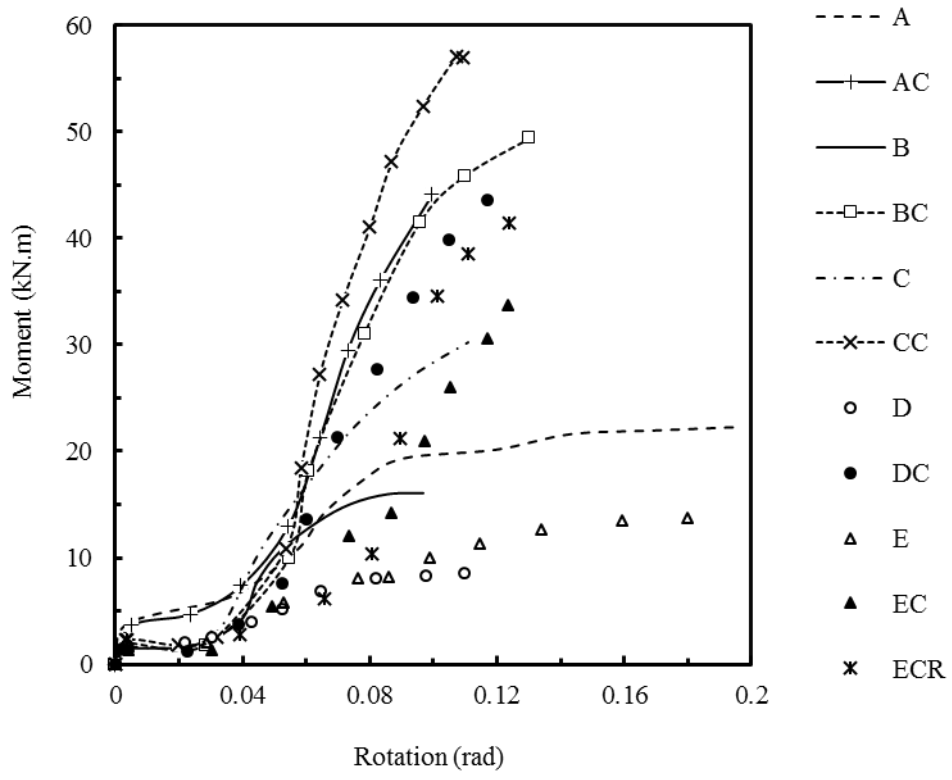

Figure 3. Summarized moment vs. rotation relationships.

Table 2. Failure moment and corresponding rotation.

Specimen ID	Failure moment kN.m	Rotation rad	M_{filled} /M_{hollow}
Joint-A	22.3	0.20	/
Joint-AC	43.8	0.11	1.96
Joint-B	16.0	0.10	/
Joint-BC	49.6	0.12	3.10
Joint-C	30.0	0.11	/
Joint-CC	57.2	0.11	1.91
Joint-D	8.4	0.12	/
Joint-DC	43.6	0.11	5.19
Joint-E	13.3	0.18	/
Joint-EC	33.8	0.13	2.54
Joint-ECR	41.4	0.13	3.11

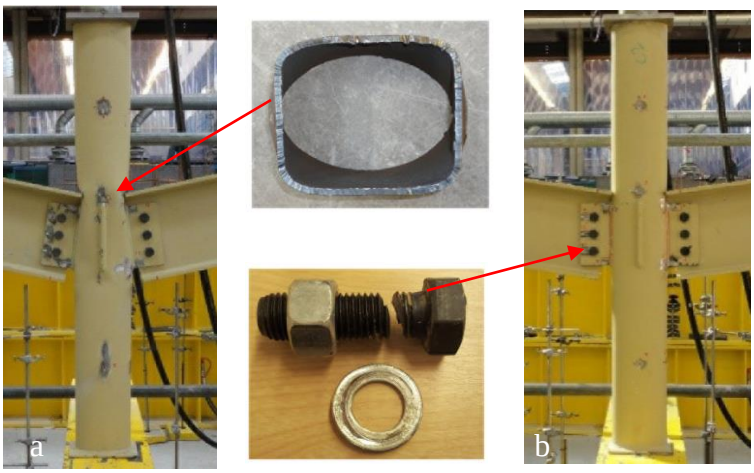

Figure 4. Typical failure modes: (a) hollow connection (Joint-A); (b) concrete-filled connection (Joint-AC)

3 **Finite element modeling method**

3.1 *Geometric model*

To achieve computational efficiency, only half of each specimen was modelled by defining appropriate symmetry in the boundary conditions. The geometric model with mesh is shown in Figure 5, including the symmetry plane and the applied loads. Mean measured dimensions of EHS columns illustrated in Table 1 were used. Bolt hole positions of both beam web and fin plates are shown in Figure 2. Note that the actual gap between end of the beam flange and the EHS column face was not exactly equal to the design value of 10 mm after assembling the connection, owing to the imperfections of the bolt hole positions and the 2 mm clearance between the bolts and the holes. Therefore, the actual gap was considered in the FE Model accordingly. The bolts were positioned in accordance to the test setup, in order to provide a more accurate simulation to the test; adopted positions were illustrated in Figure 6 as an example. Hexagonal bolt heads and nuts were simplified as cylinders in the models. This simplification was also adopted by other

researchers [10, 11]. A pre-tightening load of 20 kN was applied to each bolt of the BC, CC, DC and EC connections. Note that fillet weld and washers were not included in the FE models.

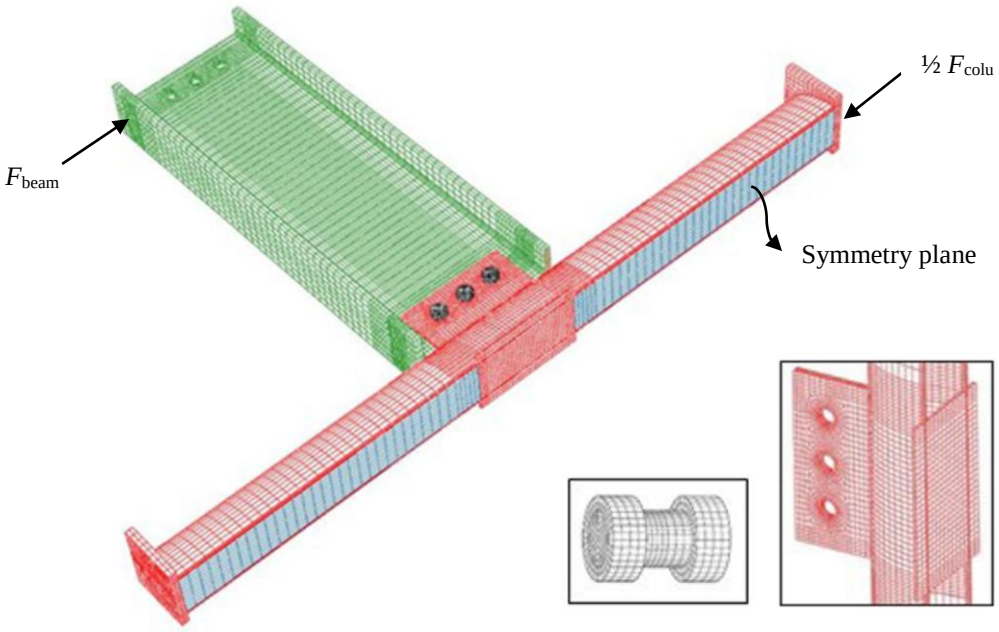

Figure 5 Finite element model with mesh (1/2 model).

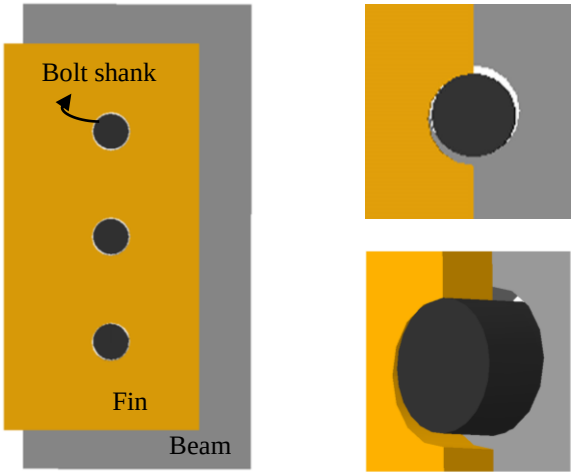

(a) Central position (b) Off center (Joint-AC)

Figure 6 Bolt positions in FE models

3.2 *Material properties*

A four part stress-strain model described by Dai & Lam [2] was adopted for the EHS confined concrete, and the calculated compressive stress-strain curve is shown in Figure 7; key parameters are listed below: maximum unconfined compressive cylinder strength was 33.2 MPa; initial elastic modulus was 30826 MPa; maximum confined compressive strength was 43 MPa. A fracture energy based option was selected to define the tensile behaviour of the concrete, with the failure stress approximately equals to 0.1 times the corresponding compressive stress and a fracture energy of 0.08

N/mm which was obtained through linear interpolation between 0.04 N/mm for C20 concrete and 0.12 N/mm for C40 concrete [12].

The stress-strain model of steel is illustrated in Figure 8 where the vertical and horizontal axes represent the true stress and strain converted from the tested nominal values via the following recognized expressions based on the principle of constant-volume:

$$\sigma^t = \sigma^n(1 + \varepsilon^n) \quad \text{(a)}$$

$$\varepsilon^t = ln(1 + \varepsilon^n) \quad \text{(b)}$$

where σ^t and ε^t denote the true stress and true strain, respectively; σ^n and ε^n refer to the nominal stress and strain. The true stress and strain at fracture are obtained by using the following equations:

$$\sigma_f = \frac{F_{frac}}{A_{frac}} \times 100\% \quad \text{(c)}$$

$$\varepsilon_f = \ln(\frac{A_0}{A_f}) \quad \text{(d)}$$

where F_{frac} and A_{frac} are the load and smallest cross-sectional area when the coupon is fully fractured; A_f is the smallest cross-sectional area after fracture. Tested σ_f and ε_f are 940.5 MPa and 96.4% for S355 steel; 943.7 MPa and 102.9% for S275 steel. As material tests for bolts were not conducted, the minimum nominal yield and ultimate strength were used in this paper.

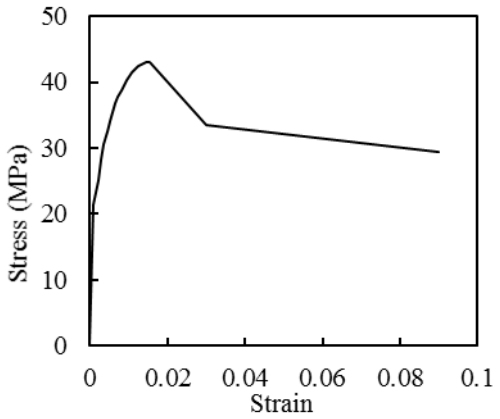

Figure 7. Stress-strain curves of EHS confined concrete (Dai & Lam, 2010).

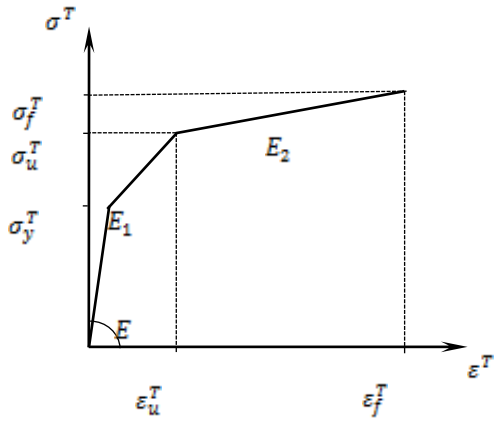

Figure 8. Stress-strain model of steel (Fernandez-Ceniceros et al, 2015).

3.3 *Mesh type and size*

C3D8, an 8-node linear brick element, was adopted for the FE model. Incompatible mode was selected for steel component elements to avoid possible hourglass phenomena while 'reduced integration' was used for the concrete core elements to reduce computational cost.

For the tested specimens, failure normally occurred around the connection, thus a finer mesh was used to obtain accurate simulation while a coarser mesh was adopted further away from the connection area to save computational time. No global buckling of the EHS column was observed during the tests, therefore the following mesh size recommendations for elliptical stub concrete-filled columns could be followed: 5-10 mm for EHS and 10-20 mm for concrete; the concrete element size could be set as twice the element size of the EHS column where applicable [2]. Also, a mesh size of 20 mm was employed for both steel and column of the through-plate concrete-filled connection [13], which gave sufficiently accurate results with quick convergence and reasonable computational time. Taking the above findings into consideration, global mesh sizes of 20mm were adopted for both the EHS and concrete core while mesh sizes of 10 mm and 5 mm were used in the connection area for concrete and EHS, respectively. The hoop direction of the EHS column was meshed using a single bias meshing method with a minimum mesh size of 10 mm (curved side of EHS) and maximum of 20 mm (flat side, this value may be reduced accordingly); the same technique was used in the longitudinal direction of the EHS column. The steel components had two layers of mesh in their thickness directions. A bolt mesh size of 3 mm was recommended by Yu et al. [14] and was thus adopted as the global size for the bolts in this paper. In particular, mesh size was minimized to 2 mm along part of the bolt shank longitudinal edges where the surface was defined as 'slave surface' in one of the contact pairs. In the circumferential direction of the bolts/bolt holes, 32 elements were adopted. Mesh sensitivity analysis was conducted in terms of this element quantity by increasing the number to 48 and 60. As shown in Figure 9 (a), the moment-rotation curves obtained are nearly identical and this proves that the FE model could adopt the 32 elements as the optimum option regarding computational efficiency and result convergence. Further evidence is given in Figure 9 (b) where the equivalent plastic strain

distribution along the critical bolt hole in fin plate (Joint AC-4mm-Fin, model details can be found in the following parametric study) was illustrated. The x-axis represents the angle initiating from 0° to 360°.

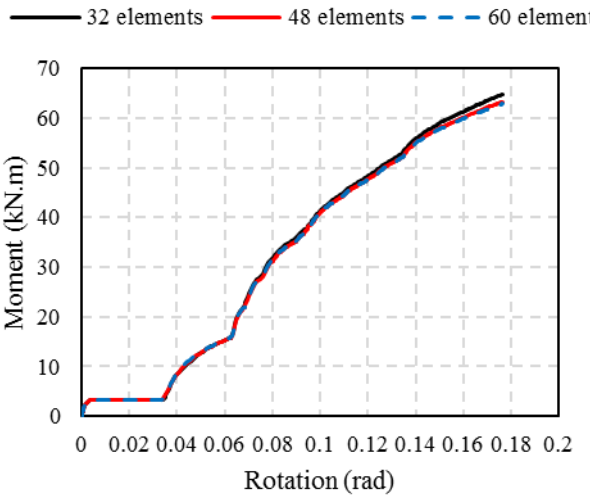

(a) Moment-rotation curves (Joint-AC)

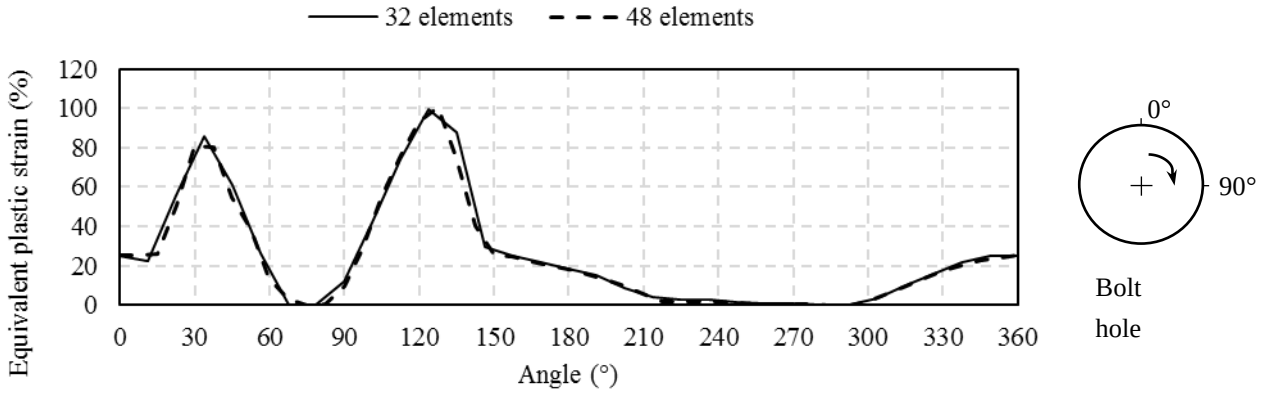

(b) Equivalent plastic strain distribution (Joint AC-4mm-Fin)

Figure 9. Mesh sensitivity analysis.

3.4 *Contact*

Contact interaction is complicated when conducting the nonlinear analysis of concrete-filled bolted connections by using the ABAQUS standard solver. Proper definitions of master and slave surfaces in contact pairs (in accordance with the below two criteria: 1) stiffer material is normally set as the master surfaces; 2) a surface should not be used as slave surface in two or more different interactions) and contact properties were essential to avoid possible convergence problems and to successfully capture the moment-rotation behaviour of the connections. Surface-to-surface contact with a finite sliding option was used in this paper for the following contact pairs: beam-fin plate, beam/fin plate-bolt, stiffener plate/through plate-concrete, rigid plate/roller (described in the next section) -concrete, EHS-concrete. 'Hard contact' in the normal direction was defined to fully transfer the load from beam to column through fins and bolts; a friction coefficient of 0.3 was assumed for all of the contact surfaces in the tangential direction.

3.5 *Failure criteria*

The strain based failure criterion for bolted connections adopted by Salih et al [15] were employed to define the bolt shear and plate failure in the numerical studies. In this paper, bolt failure is deemed to occur when the equivalent plastic strain over the full critical cross-section of the bolt exceeds 1%. The plates bearing failure and net section failure are adopted with the criterion that the localized equivalent plastic strain reaches the true fracture strain [15] to identify the failure modes and the failure moment of the bolted connections regardless of the deformation limit of bolt holes. For the true fracture strain, experiments have been carried out by Khoo et al. [16], Dowling [17], Huns et al [18] and Nip et al [19] and an average value of 100% was obtained for structural carbon steels [15]. Based on the uniaxial tension test results of 96.4% for S355 steel and 102.9% for S275 steel obtained by authors, this value 100% is reasonable and therefore was used in the parametric studies conducted in this paper.

4 **Verification of developed FE model**

Based on the above described FE simulating method, moment vs. rotation relationships of concrete-filled connections were obtained and compared with the corresponding test results, see Figure 10 (a)-(e), where dotted lines with hollow circles represent the test results while solid lines denote the corresponding FE results; the dotted line with filled circular data points and the thicker dashed line in Figure 10 (e) refer to test result and FE result of the repeat experiment of Joint-EC (replacing Gr. 8.8 bolts by Gr. 10.9 bolts), respectively.

In general, the whole experimental moment vs. rotation curves before the maximum point (caused by bolt shear failure) can be well captured by the FE modeling with the exception of Joint-EC. The EC connection underwent yielding, along the intersection between the fin plate and the EHS column during the initial testing (see Fig. 11), however this is not considered in the FE modeling. The friction and slippage between beam and fin plate can be predicted reasonably in all specimens based on the initial stages of these moment vs. rotation curves from the FE simulation and experimental result. Nevertheless, there was a gentle transition phase in the experimental curve before the bolt shanks fully contacted the surface of the bolt holes, which was governed by bolt positions. The positions of bolts in the holes could not always locate in the center and thus real positions were used, e.g. Joint-AC (see Figure 6). Good agreement of the transition phase could be obtained for Joint-AC which means the actual bolt positions were correctly assumed. However, the bolt positions could have a number of combinations and thus leads to the differences on the moment-rotation curves at around 0.04 rad to 0.06 rad for the rest of connections. But this phenomenon will not affect the subsequent stage of the moment behaviour of the connections nor the ultimate moment capacities after beam end touching the column sides. The gap between beam end and column face affected the slope of the curve in the later stage: a smaller gap caused the slope to change at an earlier stage. The gaps used in the FE models are listed as follows: AC, 9.1 mm; BC, 9 mm; CC, 8.5 mm; DC, 7 mm; EC, 12mm, ECR, 11mm.

Figure 12 shows the equivalent plastic strain distribution along the critical bolt hole in both the fin plate and the beam web of Joint-AC when bolt failure occurred. The data points were extracted in a clockwise direction with the angle initiating from 0° to 360°. It indicates that the connection did not fail by plate failure since the maximum equivalent plastic strain (around 40%) is below the limit of 100%.

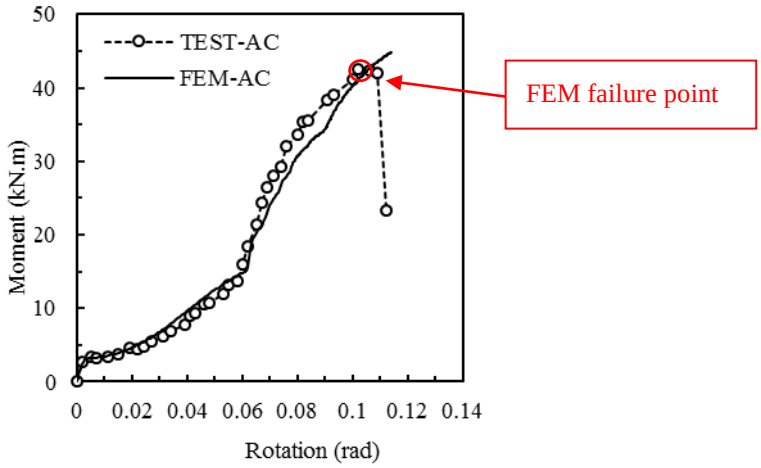

(a) Joint-AC

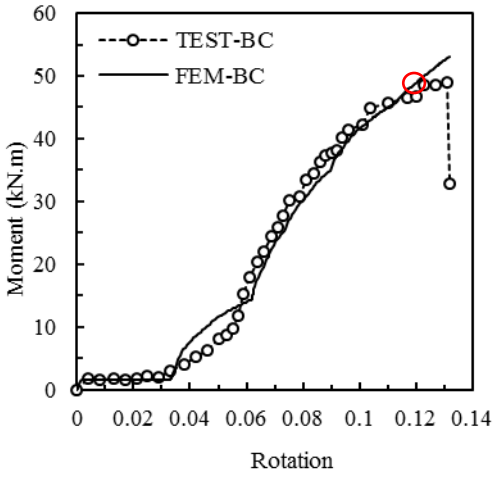

(b) Joint-BC

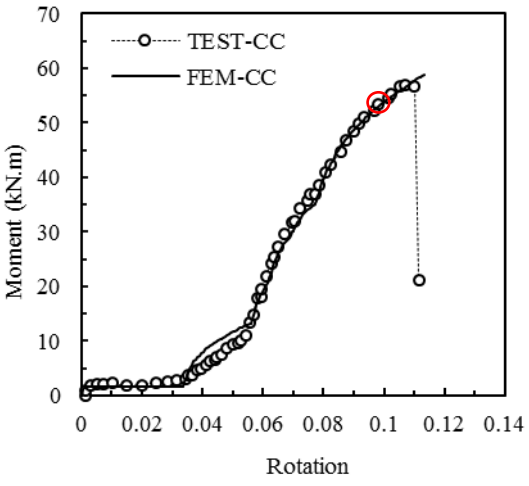

(c) Joint-CC

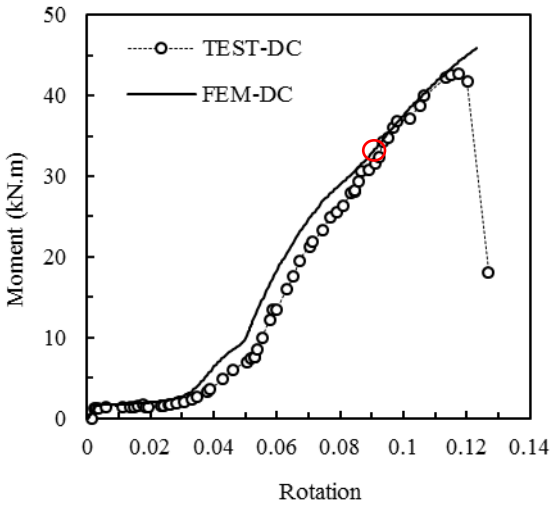

(d) Joint-DC

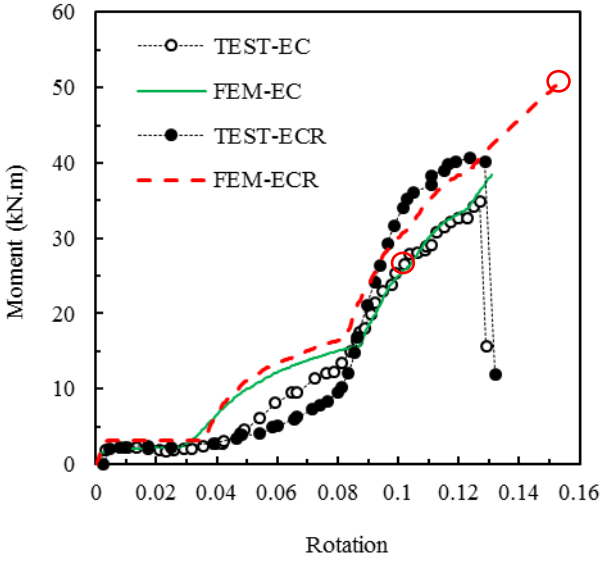

(e) Joint-EC & ECR

Figure 10. Comparisons of moment vs rotation relationships.

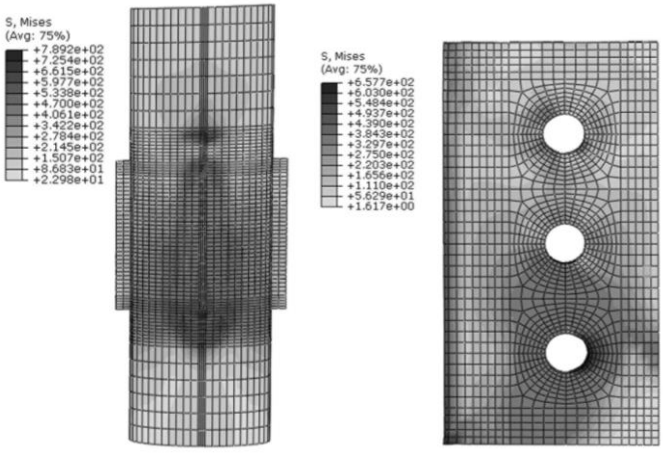

Figure 11. Von Mises contour around connection after bolt failure (Joint-EC)

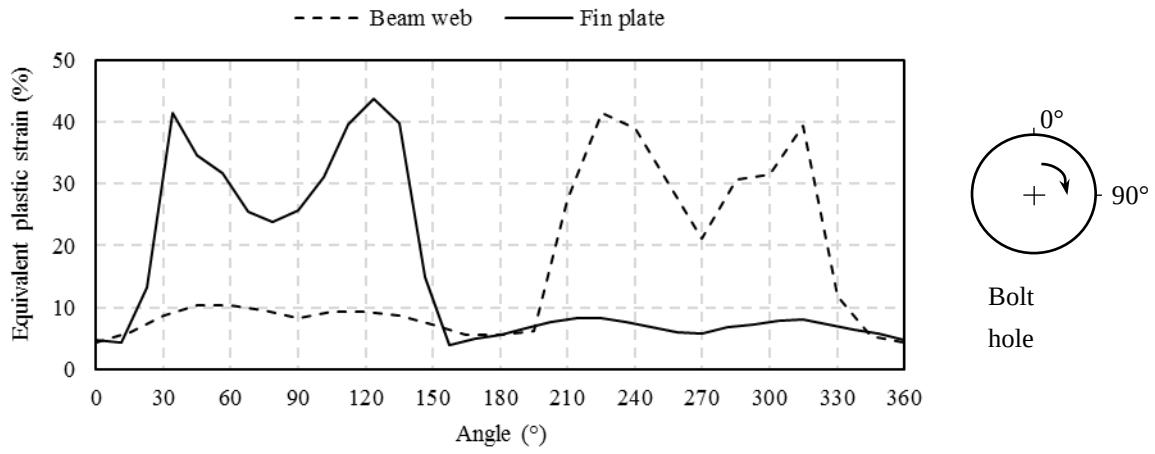

Figure 12. Equivalent plastic strain distribution at bolt failure (Joint-AC)

Figure 13 (a)-(c) shows the comparisons of typical failure modes of concrete-filled connections between experimental result and FE result, e.g. Joint-BC. As can be seen from these comparisons, the obtained FE models could reasonably replicate the failure of the connections which proves the validity of the described FE modeling method.

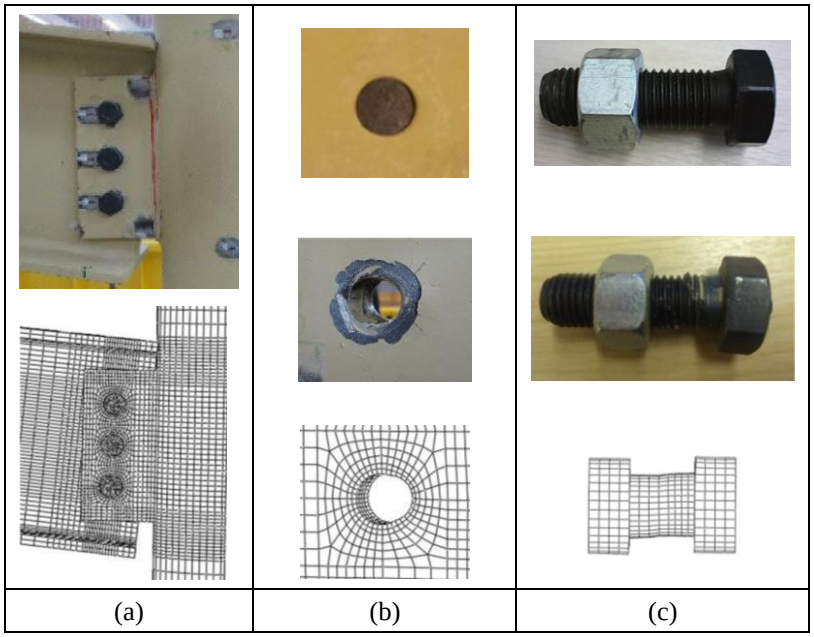

Figure 13. Comparison of failures (Joint-BC): (a) connection rotation; (b) bolt hole bearing failure in fin plate; (c) bolt shear failure (bolt deformation scale: 1.5).

Table 3 shows a comparison of ultimate moment between those extracted from experiments and FE simulation, where M_{TEST} represents the ultimate moment obtained from the experiments and M_{FEM} refers to the failure moment provided by FE simulation based on the bolt failure criteria. The failure point in the FE result was illustrated in Figure 10 with a red circle. Good agreement within a satisfied accuracy of 7% has been obtained for Joint-AC, BC and CC which utilized the Gr. 10.9 bolts which means that the developed FE model, adopted material properties and failure

criteria could reasonably determine the moment capacities of the concrete-filled connections adopting Gr. 10.9 bolts. For the cases of Joint-DC and EC in which Gr. 8.8 bolts were utilized, the simulation results are in the safe side which means the adopted bolt nominal properties and the equivalent plastic strain limit of 1% underestimated the connection capacities based on the comparison in Table 3.

Table 3. Comparison of ultimate moments from experiments and FE simulations.

Specimen ID	M_{TEST} kN.m	M_{FEM} kN.m	M_{TEST} /M_{FEM}
Joint-AC	43.8	44.5	0.98
Joint-BC	49.6	48.5	1.02
Joint-CC	57.2	53.3	1.07
Joint-DC	43.6	32.8	1.33
Joint-EC	33.8	27.6	1.23
Joint-ECR	41.4	50.6	0.82

5 **Parametric studies**

5.1 *Key parameters*

Parametric studies were performed based on the joint types-AC (major axis fin plate connection with stiffener), BC (major axis fin plate connection without stiffener) and CC (minor axis through plate connection). The key parameters selected are: end distance e_1 (1.5d, 2.0d, 2.5d, 3.0d, 3.5d), end distance e_2 (1.5d, 2.0d, 2.5d, 3.0d, 3.5d), bolt spacing p_1 (2.0d, 2.5d, 3.0d, 3.5d, 4.0d), fin plate thickness t_p (4mm, 6mm, 8mm); d is the diameter of the bolt which equals to 20mm. Symbols are illustrated in Figure 2. Dimensions of the beams, EHS column are identical with those adopted in the experiments. The column end was fixed on the bottom while only axial shortening was allowed at the top end. Three Gr. 10.9 bolts were adopted with a constant diameter of 20mm. The beam flange and fin plate/through plate was tightened with bolt load of 20 kN. No weld and washers are included in the FE models.

S355 steel was adopted for the EHS columns and beams with a nominal yield strength of 355MPa and a nominal minimum ultimate strength of 470MPa [20] while S275 steel was selected for the fin plates which has a nominal yield strength of 275MPa and nominal minimum ultimate strength of 410MPa. True stress-strain relationships were converted using the equations where $E_2=\sigma_u$ was assumed [21]. The three-part linear stress-strain curve was adopted for steel. C30 concrete was used in the EHS columns.

5.2 *Effect of fin plate thickness*

To evaluate the influence of fin plate thickness on the moment-rotation behaviour and failure modes of the beam to concrete-filled elliptical column connections, a set of thickness values of 4mm, 6mm and 8mm was selected for Joint types-AC, BC and CC. Bolt arrangement and fin plate profile can be found in Figure 2. The maximum moment with corresponding joint rotation at failure were extracted from the numerical results and are listed in Table 4. Figure 14 shows

the equivalent plastic strain distribution along the critical bolt hole in both fin plate and beam web where the x-axis represents the angle initiating from 0° to 360°. This figure indicates that the critical position along bolt hole in the beam web and fin plate is around 120°-135°. Note that the connections with fin plate thickness of 4mm and 6mm failed in fin plate failure since the equivalent plastic strain at the critical position reached the limit of 100% (highlighted with a red dash line in the graph) while the bolts did not fail as the shear resistance of M20 Grade 10.9 bolts was larger than the fin plate bearing resistance. In contrast, bolt shear failure occurred prior to the fin plate failure in the connection with 8mm fin plate and evidence was shown in the Figure 14 that the critical equivalent plastic strain is lower that the strain limit of 100%. An equivalent plastic strain contour was illustrated in Figure 15, showing that local failure in the fin plate occurred in this case and thus the stiffener plate inserted into the concrete-filled column of type-AC connection could not provide obvious enhancement to the resistance on the connection level. Thus there would be no significant difference in the moment response between the stiffened type-AC connections and type-BC connections. The moment vs. rotation curves of the connections considered in this section are illustrated in Figure 16 where the curves were cut at the failure points to clarify the comparisons within the graph. Obviously, the fin plate thickness plays important role in the structural performance of these types of connections. The stiffness and ultimate moment of the connections increase with the increasing of fin plate thickness even through failure mode might change. The connections analyzed in this section was summarized in Table 4 with the failure moment, corresponding rotation and failure mode; failure points are given in Figure 16 with circles for type-CC connections and triangles for both AC and BC connections.

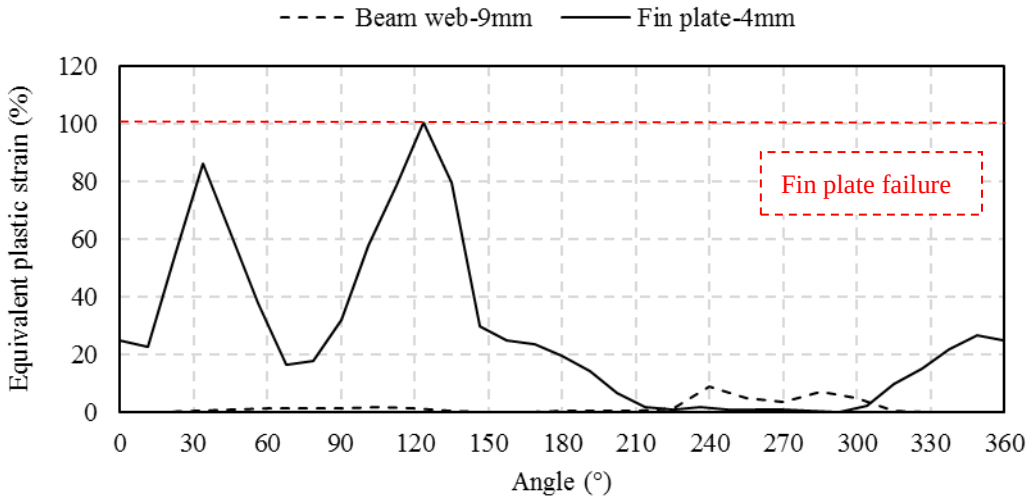

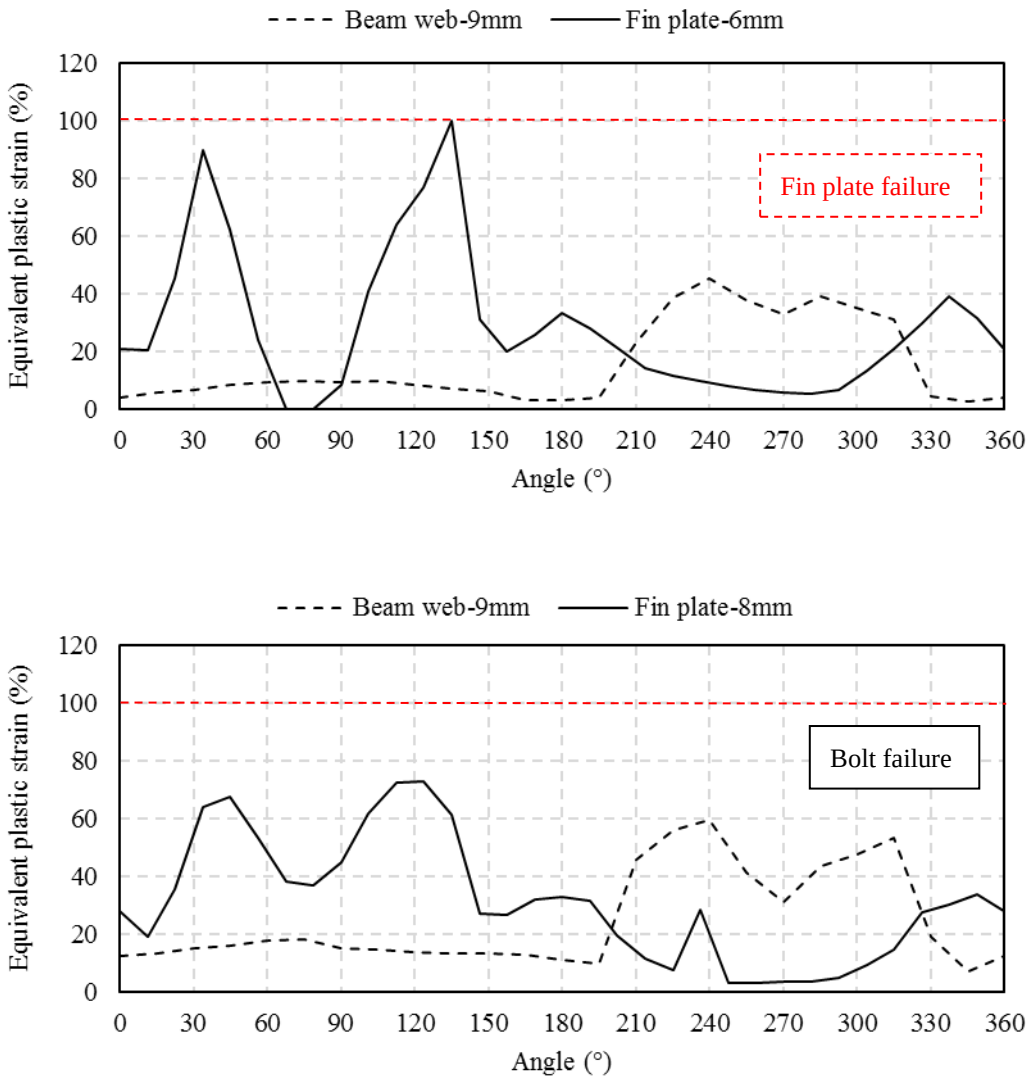

Figure 14. Equivalent plastic strain distribution along the side bolt hole at failure (AC).

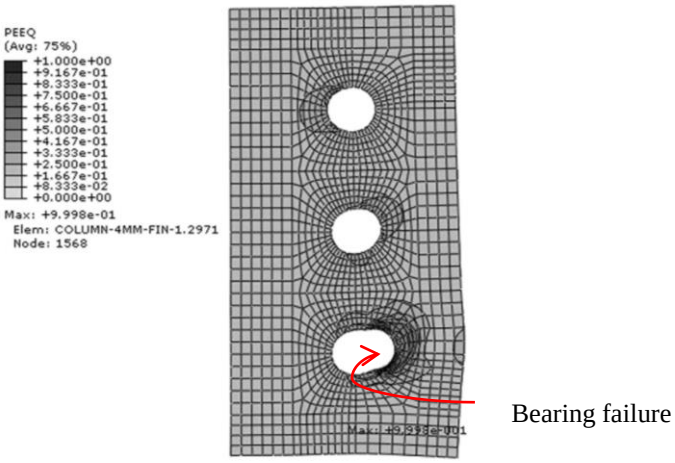

Figure 15. Equivalent plastic strain contour in fin plate (AC-4mm-Fin).

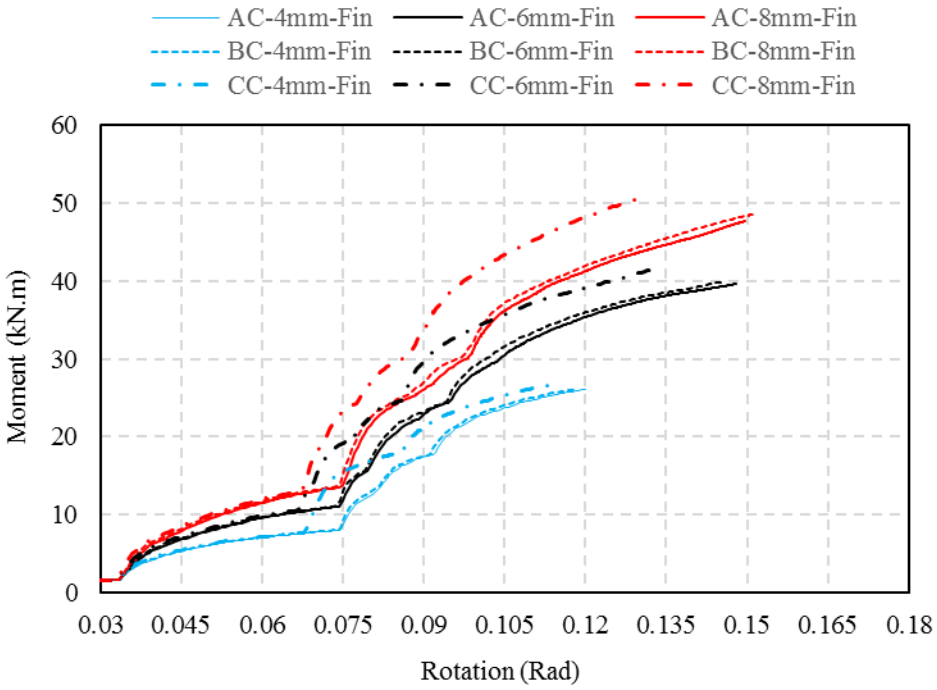

Figure 16. Moment vs. rotation relationships.

Table 4. List of beam to elliptical connections analyzed in section 5.2.

Connection ID	n_l	t_p	Failure moment	Rotation at failure	Failure mode
	mm	mm	kN.m	Rad	
AC-4mm-Fin	0.4	4	26.08	0.120	PF
AC-6mm-Fin	0.4	6	39.63	0.148	PF
AC-8mm-Fin	0.4	8	47.66	0.150	BF
BC-4mm-Fin	0.4	4	26.11	0.118	PF
BC-6mm-Fin	0.4	6	39.95	0.146	PF
BC-8mm-Fin	0.4	8	48.58	0.151	BF
CC-4mm-Fin	0.4	4	26.72	0.114	PF
CC-6mm-Fin	0.4	6	41.70	0.134	PF
CC-8mm-Fin	0.4	8	50.78	0.131	BF

Note: Connection ID, e.g. AC-4mm-Fin denotes type-AC connection with a 4mm fin plate;

BF - bolt failure and PF - fin/through plate failure.

5.3 *Effect of end distance-e_1 and bolt spacing-p_1*

Optimum arrangement of the bolts in the fin plate (110mm in width and 220 mm in length) was investigated by changing the end distance e_1 and vertical bolt spacing p_1. Considered combinations of e_1 and p_1 are given as follows: 1.5d & 4.0d; 2.0d & 3.5d; 2.5d & 3.0d; 3.0d & 2.5d; 3.5d & 2.0d. Ultimate moment capacities obtained from type-BC and CC FE models are presented in Figure 17 and are also summarized in Table 5. It is shown that bolt spacing p_1 is more influential than the end distance e_1 on the moment capacities of the connections. Based on the comparison within and between graphs, vertical bolt spacing is suggested to be at least 2.5d; the minimum e_1 could be 1.5d in type-BC connection but this value should be increased to 2.0d in type-CC connection; and the combination of e_1=2.0d and p_1=3.5d may be the optimum option for the bolts arrangement in the cases studied.

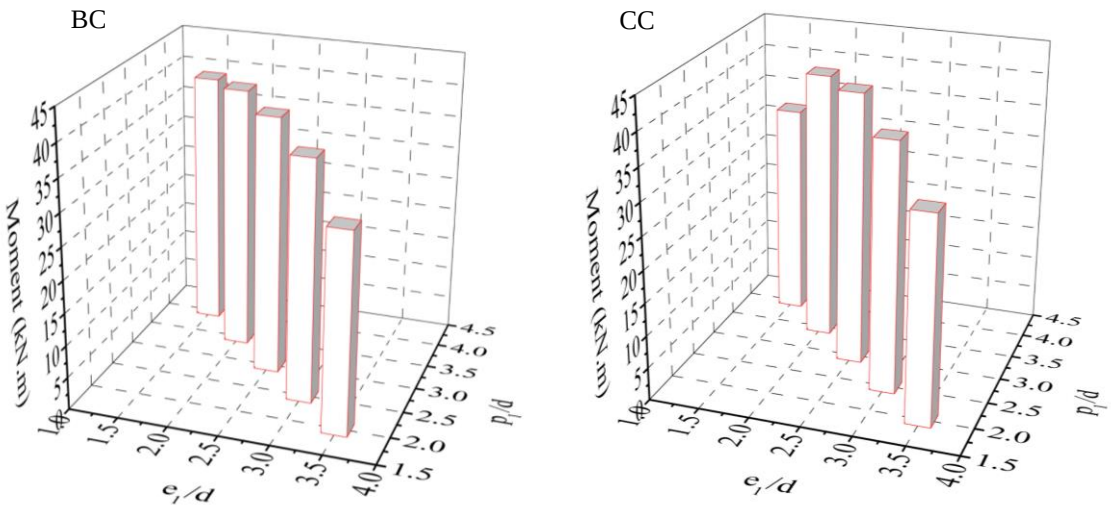

Figure 17. Effect of end distance e_1 and bolt spacing p_1 (type-BC and CC)

Table 5. List of beam to elliptical connections analyzed in section 5.3 (e_2=2.5d)

Connection ID	n_l	t_p	Failure moment	Rotation at failure	Failure mode
	mm	mm	kN.m	Rad	
BC-6-E1-15-P1-40	0.4	6	39.63	0.125	PF
BC-6-E1-20-P1-35	0.4	6	40.81	0.135	PF
BC-6-E1-25-P1-30	0.4	6	39.95	0.146	PF
BC-6-E1-30-P1-25	0.4	6	37.36	0.146	PF
BC-6-E1-35-P1-20	0.4	6	30.85	0.130	PF
CC-6-E1-15-P1-40	0.4	6	32.67	0.111	PF
CC-6-E1-20-P1-35	0.4	6	41.32	0.116	PF
CC-6-E1-25-P1-30	0.4	6	41.84	0.134	PF
CC-6-E1-30-P1-25	0.4	6	38.31	0.134	PF
CC-6-E1-35-P1-20	0.4	6	31.79	0.124	PF

5.4 *Effect of edge distance-e_2*

Figure 18 presents the moment capacities of analyzed BC and CC connections in terms of edge distance e_2. The studied e_2 values were equal to 1.5d, 2.0d, 2.5d, 3.0d and 3.5d, respectively, and the corresponding fin plate width was (60 + e_2) mm while the length is kept as 220 mm. Table 6 lists the corresponding FE results the connections. As shown from the results, the moment capacities increased with the increasing of the edge distance e_2 while the increment was not obvious after e_2 reaching 3d; the difference between the ultimate moments between connection types BC and CC is not significant but the capacity of the CC connection is always slightly bigger than that of the BC connection. The minimum value of e_2 is suggested to be at least 2.5d in both cases.

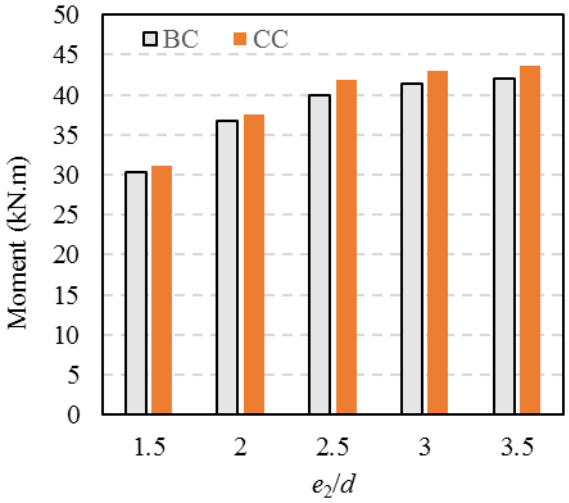

Figure 18. Effect of end distance e_2

Table 6. List of beam to elliptical connections analyzed in section 5.4 (e_1=2.5d; p_1=3d).

Connection ID	n_l	t_p	Failure moment	Rotation at failure	Failure mode
	mm	mm	kN.m	Rad	
BC-6-E2-15	0.4	6	30.30	0.119	PF
BC-6-E2-20	0.4	6	36.75	0.135	PF
BC-6-E2-25	0.4	6	39.95	0.146	PF
BC-6-E2-30	0.4	6	41.33	0.148	PF
BC-6-E2-35	0.4	6	42.03	0.147	PF
CC-6-E2-15	0.4	6	31.13	0.111	PF
CC-6-E2-20	0.4	6	37.6	0.122	PF
CC-6-E2-25	0.4	6	41.84	0.134	PF
CC-6-E2-30	0.4	6	42.96	0.134	PF
CC-6-E2-35	0.4	6	43.55	0.132	PF

6 **Conclusions**

To enable better understanding of the moment-rotation behaviour and failure mechanism of fin plate connections to elliptical column, limited experimental work has been conducted by authors. Due to experiment is costly and time consuming, a finite element modelling method was develped via ABAQUS and was adopted to conduct further investigation. After the developed numerical model was validated against the experimental results, a preliminary parametric study is then performed to evaluate the influence of several main parameters to the behaviour of the prescribed connections. The following conclusions are made based on the research work presented in the paper.

- The concrete core increased the moment capacity significantly due to it restrained the column wall buckling at the vicinity of the joint. The moment enhancement ratio ranging from 1.91 to 5.19 (compared with corresponding hollow connections);

- Typical failure of the concrete-filled connections was observed as bolt shear failure while that of the hollow connections was inwards local buckling, which occurred in compression zone of the EHS column face near the connection area.
- Based on the comparisons between experimental result and FE analysis prediction, the described simulation method/FE model could predict the ultimate moment capacity of concrete-filled connections adopting M20 Gr. 10.9 bolts within a satisfactory error value of 7 % and could also capture the typical failure mode of these connections.
- The numerical results obtained from the parametric studies indicates that the fin plate thickness affects the moment capacity of the connections significantly. Normally, the ultimate moment increases with the increasing of the fin plate thickness although the failure mode may change when the thickness reaches a certain value, e.g. 8 mm.
- Vertical bolt spacing is suggested to be at least 2.5d for both type-BC and CC connections; the minimum e_1 could be 1.5d in type-BC connection and 2.0d in type-CC connection. The minimum value of e_2 is suggested to be at least 2.5d in both cases.

7 References

[1] Zhao XL, Packer JA. Tests and design of concrete-filled elliptical hollow section stub columns. Thin-Walled Structures. 2009;47:617-28.

[2] Dai X, Lam D. Numerical modelling of the axial compressive behaviour of short concrete-filled elliptical steel columns. Journal of Constructional Steel Research. 2010;66:931-42.

[3] Law KH, Gardner L. Lateral instability of elliptical hollow section beams. Engineering Structures. 2012;37:152-66.

[4] Shen W, Choo YS, Wardenier J, Packer JA, van der Vegte GJ. Static strength of axially loaded EHS X-joints with braces welded to the narrow sides of the chord. Journal of Constructional Steel Research. 2013;88:181-90.

[5] Shen W, Choo YS, Wardenier J, Packer JA, van der Vegte GJ. Static Strength of Axially Loaded Elliptical Hollow Section X Joints with Braces Welded to Wide Sides of Chord. I: Numerical Investigations Based on Experimental Tests. Journal of Structural Engineering. 2014;140:04013035.

[6] Jones MH. Tensile and Shear Behaviour of Fin-plate Connections to Hollow And Concrete-filled Steel Tubular Columns At Ambient And Elevated Temperatures. PhD Thesis, University of Manchester. 2008.

[7] Lam D, Dai X. Finite Element modelling of beam to concrete filled elliptical steel column connections. Tubular Structures XIV Gardner (Ed). 2012;Taylor and Francis Group, London, ISBN 978-0-415-62137-3:289-96.

[8] Yang J, Sheehan T, Dai XH, Lam D. Experimental study of beam to concrete-filled elliptical steel tubular column connections. Thin-Walled Structures. 2015;95:16-23.

[9] CEN. Metallic materials-tensile testing-Part1: Method of test at ambient temperature. EN ISO 6892-1: 2009. 2009.

[10] Sarraj M, Burgess IW, Davison JB, Plank RJ. Finite element modelling of steel fin plate connections in fire. Fire Safety Journal. 2007;42:408-15.

[11] Wang J, Spencer BF. Experimental and analytical behavior of blind bolted moment connections. Journal of Constructional Steel Research. 2013;82:33-47.

[12] Han LH. Concrete-filled steel tubular structures-theory and practice (2nd ed.). Beijing: China Science Press (in Chinese). 2007.

[13] Mollazadeh MH, Wang YC. New insights into the mechanism of load introduction into concrete-filled steel tubular column through shear connection. Engineering Structures. 2014;75:139-51.

[14] Yu H, Burgess IW, Davison JB, Plank RJ. Numerical simulation of bolted steel connections in fire using explicit dynamic analysis. Journal of Constructional Steel Research. 2008;64:515-25.

[15] Salih EL, Gardner L, Nethercot DA. Numerical investigation of net section failure in stainless steel bolted connections. Journal of Constructional Steel Research. 2010;66:1455-66.

[16] Khoo HA, Cheng RJJ, Hrudey TM. Ductile fracture of steel. Structural engineering report no. 233. Canada: Department of Civil & Environmental Engineering, University of Alberta. 2000.

[17] Dowling NE. Mechanical behaviour of materials. New Jersey: Prentice Hall. 1999.

[18] Huns BB, Grondin GY, Driver RG. Block shear behaviour of bolted gusset plates. Structural engineering report no 248 Canada: Department of Civil & Environmental Engineering, University of Alberta. 2002.

[19] Nip KH, Gardner L, Davies CM, Elghazouli AY. Extremely low cycle fatigue tests on structural carbon steel and stainless steel. Journal of Constructional Steel Research. 2010;66:96-110.

[20] CEN. Hot finished structural hollow sections of non-alloy and fine grain steels-Part 1: Technical delivery conditions. EN 10210-1:2006(E), European Committee for Standardization, Brussels, Belgium. 2006a.

[21] Fernandez-Ceniceros J, Sanz-Garcia A, Antoñanzas-Torres F, Martinez-de-Pison FJ. A numerical-informational approach for characterising the ductile behaviour of the T-stub component. Part 1: Refined finite element model and test validation. Engineering Structures. 2015;82:236-48.